Article:
Dong, B., Jacas Biendicho, J., Hull, S. et al. (2018) In-Situ Neutron Studies of Electrodes for Li-Ion Batteries Using a Deuterated Electrolyte: LiCoO2 as a Case Study. Journal of The Electrochemical Society, 165 (5). A793-A801. ISSN: 0013-4651

https://doi.org/10.1149/2.0291805jes

In-situ neutron studies of electrodes for Li-ion batteries using a deuterated electrolyte; $LiCoO_2$ as a case study

Bo Dong[1,2], Jordi Jacas Biendicho*[3], Stephen Hull[1],
Ronald I. Smith[1], and Anthony R. West[2].

1. Crystallography Group, The ISIS Facility, STFC Rutherford Appleton Laboratory, Chilton, Didcot, OX11 0QX, United Kingdom.
2. Department of Materials Science and Engineering, University of Sheffield, Sheffield, S1 3JD, United Kingdom.
3. Catalonia Institute for Energy Research, Jardins de les Dones de Negre 1, 08930 Sant Adrià de Besòs, Spain.

*Corresponding author: jjacas@irec.cat

Abstract.

An electrochemical cell for in-situ neutron powder diffraction studies of electrode materials for lithium-ion batteries is presented. The device has a coin cell geometry, consisting of 8.4 cm diameter, circular components that can be stacked together and clamped tight using sixteen polyetheretherketone (PEEK) screws. The background issue associated with incoherent scattering from hydrogen within the organic electrolyte was addressed by replacing the normal electrolyte with a deuterated analogue, significantly improving the peak-to-background ratio of the in-situ neutron data. Initial in-situ studies showed clear structural evolution within Li_xCoO_2 during charge in a half-cell with lithium metal as the counter electrode, in agreement with previous studies. In addition, the in-situ cell was shown to provide electrochemical performance comparable to that of equivalent coin cells of the commercial design and, following these demonstration studies, is available for in-situ structural studies of other lithium cathode and anode materials during charge/discharge cycling.

1. Introduction.

1.1. Lithium-ion Batteries.

The world's energy demands are likely to be doubled to 28TW by 2050, largely due to global population growth [1]. In order to suppress CO_2 emissions and minimize global warming effects, energy must increasingly be provided by greener resources, such as solar and wind, rather than fossil fuels. This, in turn, requires the development of sustainable energy storage technologies.

Since the development of the first commercial cells using a carbon anode and a $LiCoO_2$ cathode by Sony in 1991 [2], lithium-ion batteries have attracted considerable interest, because their combination of high specific energy and specific power makes them uniquely suitable for portable energy storage systems. Indeed, lithium-ion batteries are a suitable energy storage technology to contribute more widely to an energy sustainable economy, including electric vehicles (EV) and grid applications of energy harvesting. However, the increasing market demands provide a relentless challenge to develop new electrode materials with still higher energy and power densities, longer cycle life, minimal environmental impact and lower cost. In parallel, safety issues arising from the use of flammable organic liquid electrolytes provide a strong motivation towards the development of either ionic liquids [3, 4] which are safer or solid electrolyte materials for use in all solid state batteries [5].

Capacity fading in Li-ion batteries is related to complex and interrelated processes which include chemical reactions at the particle surface in contact with the electrolyte or solid electrolyte interface (SEI) [6,7], and/or structural changes within the electrode materials [8,9]. Such issues are a direct consequence of the materials used within the current lithium-ion batteries and have motivated the use of neutron powder diffraction to probe the relationship between electrochemical performance and structural properties within the electrode materials. There are a number of reviews which provide more detailed descriptions, including those devoted to the design of in-situ electrochemical cells for neutron diffraction [10], the wider topic of neutron scattering applications to study energy related materials [11] and the use of

in-situ neutron powder diffraction studies across the broader fields of chemistry and materials science [12].

1.2. Neutron Powder Diffraction.

Powder diffraction studies, using either X-ray or neutron radiation, are extensively used to characterise the crystal structure of materials employed within technological devices and assess candidate new compounds. Neutron powder diffraction possesses a number of advantages over its X-ray counterpart, which stem from its inherent properties [13-17]. These include increased sensitivity to the locations of light atoms in the presence of heavier ones and, often, a better ability to distinguish between neighbouring atoms within the periodic table [18]. Furthermore, as the scattering power differs between different isotopes of the same element, isotopic substitution can be used to increase (or, indeed, decrease) the sensitivity of the technique to the locations of certain chemical species. The absence of a 'form factor' for neutron scattering also allows diffraction data to be collected to shorter *d*-spacings, which can be important to determine reliable information on the thermal vibration parameters and fractional site occupancies during Rietveld refinement using the diffraction data. Finally, neutron scattering is a comparatively weak process and, for most nuclei, absorption processes are insignificant. Thus, neutron powder diffraction can be used to investigate bulk samples (typically several cm^3 in size) and the penetrating power of neutrons also permits studies of samples contained within complex containment devices. This is a major factor in the development of in-situ neutron powder diffraction techniques, which form the subject of this paper.

1.3. In-situ Studies.

In recent years, there has been increasing interest in the application of neutron powder diffraction methods to probe technologically relevant materials, using in-situ cells to reproduce the conditions experienced by the sample within its application.

There are essentially two methods used to produce the intense beams of neutrons required for diffraction studies - fission of uranium within a nuclear reactor and the acceleration of protons within a synchrotron, which then bombard a heavy metal target. For in-situ powder diffraction studies, the polychromatic nature of the "white" beam produced by accelerator-based facilities has the advantage that a diffraction pattern can be collected at fixed scattering angle 2θ using the so-called 'time-of-flight' method and, in practise, large area detectors covering an extended 2θ range are generally used in order to maximize the count rate. However, in reality, the development of such specialised cells is not straightforward, as inevitably, the design process involves a compromise between the desire to collect the best possible quality of diffraction data and the need to mimic the conditions found in the technological application.

As discussed by Biendicho *et al* [19], the quality of the structural information that may be obtained during an in-situ neutron powder diffraction experiment into a battery electrode material is highly dependent on the design of the cell and the choice of its components. The typical incident flux at a neutron source is rather low, especially when compared to synchrotron X-ray sources, requiring the use of relatively large (~cm^3) sized samples. Whilst neutrons can easily penetrate metal containers, such components will produce additional Bragg peaks within the measured diffraction pattern, adding complexity to the data analysis process. For instance, aluminium diffraction peaks, as observed by Roberts *et al* [20], may be reduced by the use of aligned single crystal wafers, e.g. silicon (100), as casing material [21]. Furthermore, in order to probe the locations of H within an electrode material, it is then advisable to replace H with the isotope D if possible, to exploit its higher scattering power and significantly lower incoherent scattering cross section which, in the case of nickel metal hydride (Ni-MH) battery studies, was achieved by ex-situ cycling of the cell prior to in-situ diffraction [22]. Likewise, the amount of H within other components (*e.g.* the electrolyte) within the cell should be minimised, or replaced with deuterated analogues, if possible [23]. In this sense, a low-cost deuterated ethyl acetate based electrolyte suitable for in-situ neutron diffraction has been reported, showing comparable electrochemical performance and signal-to-noise ratio of neutron diffraction patterns to more expensive conventional deuterated electrolytes [24]. Most importantly, the electrochemical performance of the in-situ cell should

be similar to that of the real (commercial) battery, so that the structural information extracted can be directly compared to that found within the technological applications. However, this is not straightforward, since an in-situ cell design that shows a good signal-to-noise ratio of neutron diffraction patterns is usually limited to electrochemical experiments at equilibrium conditions *i.e*. slow C rates. Conversely, in-situ cells that operate at non-equilibrium conditions *i.e*. high C rates, usually show lower signal-to-noise ratios, and most often the structural information that can be obtained is limited to lattice parameter variation during charge/discharge. The compromise between electrochemical performance and diffraction pattern quality for an in-situ cell is rather complex and, for that reason, investigation of commercially available batteries by in-situ techniques has regained interest recently [25,26], even though the extracted structural information of electrode materials is limited compared to the use of specially designed in-situ cells.

1.4. In-situ Electrochemical Cells.

In-situ electrochemical cells for neutron diffraction experiments can be classified into two designs with respect to the layered sheets that build up the battery; cylindrical or planar. The first usually contains a wound laminate made up of cathode, anode, current collector and a separator sealed into a battery casing to preserve moisture- and oxygen- free conditions. A significant number of cells have been fabricated and tested with this design, following the work conducted by Bergstöm *et al* [27]. A cylindrical cell with rolled-up components is generally fabricated using printed electrodes, which ensure comparable electrochemical results to the ones obtained ex-situ at the laboratory. However, the assembly of a large cylindrical cell for in-situ experiments requires a large amount of separator. For instance, ~32 cm^2 of separator for 1 g of printed electrode. This represents a similar % in weight for both active material and separator in the case of a glass-fibre separator, which is usually preferred to Polypropylene (PP) for in-situ experiments. The large amount of separator within the cell increases the intensity of the background signal in the neutron diffraction patterns, often masking the less intense diffraction peaks of the active material. Figure 1 a) shows the in-situ cell originally presented by Bergstöm *et al* in 1998 and in b), an upgraded version with a wound-type configuration as presented by Sharma *et al* [28,29]. Other cells with similar

characteristics have been used to investigate $LiFePO_4$ [20], a perovskite-type electrode $Li_{0.18}Sr_{0.66}Ti_{0.5}Nb_{0.5}O_3$ [30] and more recently, $LiNi_{0.5}Mn_{1.5}O_4$ [31,32].

The other cell design used for in-situ neutron diffraction studies is based on a planar configuration, and basically consists of layered sheets of components stacked on top of each other. This configuration is based on the pouch or coin cell configuration commonly used for ex-situ battery testing in a laboratory, but has been adapted to in-situ neutron experiments [33, 34]. On the other hand, specially designed cells have been constructed following this configuration in order to minimize the contribution of current collectors and battery casing to the in-situ neutron diffraction patterns. Figure1 c) shows the circular in-situ cell developed by the Novák group [35] which was used to characterize $LiFePO_4$ at C/10, and reliable structural information was obtained. Other cells with a similar geometry have been used to monitor the structural changes of $LiCoO_2$ [36], $Li_{1.1}Mn_{1.9}O_4$ [37] and $LiNi_{1/3}Mn_{1/3}Co_{1/3}O_2$ [38].

As mentioned above, we have previously presented an in-situ electrochemical cell, figure 1 d), that was used for studies of both $Ni(OD)_2$ and $MmNi_{3.6}Al_{0.4}Mn_{0.3}Co_{0.7}$ electrodes, where Mm refers to mischmetal, in a Ni-MH battery [22]. The results were interesting, since structural information obtained as a function of battery charge/discharge showed that the largest amount of deuterium contained at the positive electrode de-intercalates as a continuous solid solution, rather than by a phase transformation of the hexagonal $Ni(OH)_2$ phase as commonly observed by ex-situ measurements. The cell demonstrated comparable electrochemical performance to commercial Ni-batteries and afforded good diffraction patterns in relatively short data collection times. Furthermore, due to its modular configuration, we anticipated that other energy systems could be investigated with only minor modifications of the components that built up the cell. In this paper, therefore, we have investigated the potential application of our design to characterize a Li-based electrode, more specifically $LiCoO_2$. The aim is to broaden the spectrum of materials and/or energy which can be investigated by the in-situ cell and make it more widely available for users of the POLARIS diffractometer at the ISIS neutron spallation source.

2. Experimental.

2.1. In-situ Electrochemical Cell Design.

The electrochemical cell used for in-situ neutron diffraction has a planar design and has been presented previously [19]. It consists of 84 mm diameter circular disk-type components: two stainless steel clamp rings, two nickel metal windows, two thin nickel metal sheets, one separator module and one boron nitride shield. The cell is assembled and stacked using the sequence from right hand to left hand shown in figure 2*a*. Rear and front views of the assembled cell with respect to an incident neutron beam are also shown in figures 2*b* and 2*c*.

The main body of the cell is constructed of nickel metal and stainless steel alloy rings clamped each side of the cell, together using 16 polyetheretherketone (PEEK) screws (figure 2). The front and back windows of the cell are constructed using nickel metal (1mm thick, 99.99% purity) with an aperture of 20 mm width × 40 mm height, this being chosen as typical of the dimensions of the neutron beam commonly found on neutron powder diffractometers. The windows hold nickel metal sheets of around 0.1 mm thickness in place, which hold the electrode materials and act as current collectors. The choice of nickel metal for this component follows from its relatively simple diffraction pattern, which minimises the number of Bragg reflections contaminating the measured diffraction pattern from the in-situ cell. In principle, vanadium is a potentially useful metal for use in neutron powder diffraction studies, as its very low coherent scattering cross section gives rise to only weak Bragg peaks. However, its relatively high incoherent scattering cross section contributes to an increased background level across the entire diffraction pattern. Furthermore, nickel has the advantage of good chemical compatibility with a wide range of liquid electrolytes. The central part of the cell is a 2mm thick insulating separator module with an aperture of the same dimensions as the neutron window, which separates the nickel sheets so as to avoid a short circuit. The separator module is made of polyoxymethylene, in view of its good chemical resistivity to most commonly used liquid electrolytes. The free volume inside the module provides the main chamber of the cell, which is filled with cathode, anode and separator. O-rings seals are

located in circular grooves on each side of the separator module to avoid leakage of the organic electrolyte. Finally, a shield manufactured from boron nitride ceramic is placed at the front of the cell, exploiting the high thermal neutron absorption cross-section of boron to prevent any part of the incident neutron beam from striking the stainless steel clamp rings or the PEEK screws[18].

2.2. POLARIS instrument.

In-situ neutron diffraction data were collected at the Polaris diffractometer [39] at ISIS. Whilst the diffractometer has detector banks covering a wide range of scattering angles (2θ), the geometry of the cell means that the best quality diffraction data are collected in two of the five detector banks - low angle ($40^{\circ} \leq 2\theta \leq 67^{\circ}$, $d_{max} = 7$ Å) and backscattering ($135^{\circ} \leq 2\theta \leq 168^{\circ}$, $d_{max} = 2.7$ Å). Diffraction data were analysed by the Rietveld method using the GSAS least-squares refinement software [40]. The Bragg peak profile was described using function 3 in GSAS (a convolution of a pseudo-Voigt and two back-to-back exponential functions) and only the components of the Gaussian part of the pseudo-Voigt function were refined.

2.3. Lithium Cobalt Oxide, Li_xCoO_2.

The lithium cobalt oxide, $LiCoO_2$, used as cathode material for in-situ neutron experiments was purchased from Sigma Aldrich. It adopts a rhombohedral crystal structure (space group $R\bar{3}m$), with alternating layers of Co and Li located between close packed layers of oxygen anions [41-44], During electrochemical charge/discharge, Li^+ ions are deintercalated/intercalated and diffuse to the counter electrode through a separator whilst electrons are transported through an external circuit to provide the electrical power. This process is reversible, so energy is stored/released during the charge/discharge processes. The charge/discharge reaction at the positive $LiCoO_2$ electrode is shown below;

$$LiCoO_2 \leftrightarrow Li_{1-x}CoO_2 + xLi^+ + xe^- \quad (1)$$

2.4. Electrode and Separator Fabrication.

The cathode materials for the in-situ electrochemical tests were prepared in three different ways. Firstly, Polyvinylidene fluoride (PVDF) binder was dissolved into 1-Methyl-2-Pyrrolidinone (NMP) using a magnetic stirrer at 80 ^{o}C for 2 hr before the transfer of the $LiCoO_2$ and carbon into NMP to form a slurry. The slurry was then printed onto an aluminium foil or a nickel mesh. Secondly, $LiCoO_2$, carbon and PVDF were mixed using a mortar and pestle for 30 mins before pressing into a pellet using either a 10 mm diameter circular die or a 18 mm × 36 mm rectangular die. Finally, $LiCoO_2$ and carbon were dissolved in isopropanol and ball-milled for 12 hr to achieve homogeneity before drying in a vacuum oven at 80 ^{o}C to evaporate the isopropanol. In all cases, the final drying stage was performed in a vacuum oven at 120 ^{o}C for 10 hr. As $LiCoO_2$ adopts a rhombohedral layered crystal structure, there is the possibility that it might show preferred orientation when pressed into the ~1mm thick sheets. However, there is no evidence for this tendency in the neutron powder diffraction patterns (*i.e*. no increased intensity of (*hkl*) Bragg reflections with a strong *l* component). The separator foils were cut into 26 mm × 46 mm (PP, PTFE) and 20 mm × 40 mm (glass fibre) pieces. The lithium metal anode was handled inside a glove box, cut into pieces of 0.38 mm thickness and scratched to give a shiny surface.

2.5. Electrolyte Preparation.

Electrolyte preparation was carried out inside a glove box in order to obtain a low oxygen and water content, which is beneficial to prevent side reactions during the operation of the batteries. The cell was assembled in the glove box and only removed once sealed. Stoichiometric lithium hexafluorophosphate ($LiPF_6$) and lithium bis(fluorosulfonyl) imide (LiFSI) were weighed with a balance before normal (hydrogeneous) or deuterated propylene carbonate (PC) / ethylene carbonate (EC) / dimethyl carbonate (DMC) / ethyl acetate (EA) were added with a syringe. The lithium salts and organic solvent were transferred into a plastic jar and mixed using a magnetic stirrer for 24 hr. A number of different electrolytes were prepared and tested. In the hydrogenous electrolyte case, these were 1M $LiPF_6$ in PC,

1:2 (n/n) of LiFSI in EA and a commercial LP30 electrolyte of 1M $LiPF_6$ in 50:50 (v/v) EC/DMC. Additional tests with deuterated electrolytes used 1:2 (n/n) of LiFSI and d_8-EA.

2.6 Electrochemical tests.

A large number of ex-situ tests were performed using different Li metals, separators, carbons, graphite and carbon black ratios and various quantities of active materials and the electrolytes mentioned above. In addition, the influence of the nickel mesh, PVDF and different cathode fabricating methods were tested in order to optimise the electrochemical performance of the in-situ cell. Electrochemical tests were conducted either using a versatile multichannel potentiostat (VMP, Perkin-Elmer, U.K.) or a Bio-Logic SP-240. The EC-Lab software was used to control and analyse the collected electrochemical data.

3. Results and Discussion.

3.1. Electrochemical results

Ex-situ electrochemical tests of the cell showed that the best electrochemical performance was found with 1g of a mixture of $LiCoO_2$, graphite and carbon black in the ratio 89:3:8, a Whatman GF/D glass fibre separator, a 0.38mm thick lithium metal anode and 1.5ml of 1M $LiPF_6$ EC/ DMC electrolyte. The electrochemical performance of the cell was compared with that of a standard coin cell constructed using the same battery components, and results are shown in figure 3 a). The charge/discharge profile of the in-situ cell shows a slightly higher over potential both during charge and discharge, and its discharge capacity is lower compared to the one obtained by standard coin-cell assembly. This is expected because of the large amount of electrode material within the in-situ cell in the form of a pellet of mass ~1 gr. Maximizing the amount of active material in the cell is motivated by the need to improve the signal-to-noise ratio of the neutron diffraction patterns collected during preliminary ex-situ neutron tests. Hence, for in-situ measurements conducted at ISIS using a normal electrolyte, the cell was galvanostatically charged at C/20 with a cut-off voltage up to 4.8 V in order to

observe the maximum number of phase transitions at the positive electrode while neutron diffraction patterns were collected every 10 min (corresponding to 0.00833 Li+ per dataset).

In the case of measurements using deuterated electrolyte, there were no preliminary ex-situ tests due to the high cost of electrolyte components and these were only assembled for in-situ experiments. Figure 3 b) shows the charge profile of the cell recorded during in-situ measurement and, again, the profile corresponds to the one typically observed for $LiCoO_2$ during charge. In order to compensate for the slightly lower conductivity of the deuterated electrolyte *i.e.* LiFSI in d_8-EA, compared to the normal one *i.e.* 1M $LiPF_6$ EC/ DMC, the in-situ cell was charged at a slightly lower C-rate (C/25) and with a cut-off voltage increased to 5 V. The neutron diffraction patterns were recorded every 10 min, corresponding to $0.00667Li^+$ per dataset.

3.2 The effect of deuterated electrolyte

To demonstrate the effects of using a deuterated electrolyte, figure 4 shows neutron diffraction patterns of $LiCoO_2$ contained within a standard cylindrical sample can and cells assembled with normal (hydrogenous) and deuterated electrolytes. It is clear that the use of deuterated electrolyte dramatically decreases the background, leading to a significant increase in the peak-to-background ratio. Indeed, the statistical quality of the neutron diffraction data from $LiCoO_2$ collected from the in-situ cell with deuterated electrolyte is comparable to that collected from the sample in a vanadium can. Furthermore, due to the high symmetry of the crystal structure of nickel, Ni diffraction peaks arising from the casing/current collector do not occupy a significant portion of the powder diffraction pattern, so electrode materials with lower symmetry than $LiCoO_2$ could potentially be investigated in-situ using the cell, with minimum peak overlap.

Figure 5 compares the in-situ diffraction data collected from cells assembled with deuterated electrolyte and normal (H) electrolyte for the same collection time *i.e.* 10 min. The significantly lower background in the case of the former is clear, and emphasises that, in practice, the choice of liquid electrolyte has the major role in providing the best possible data

quality. The advantage is most clearly seen at *d*-spacings beyond around 2Å where a number of weaker Bragg reflections are more clearly seen when using the deuterated electrolyte. Allowing for the differing quality of the two sets of diffraction data, and the slight difference in charging rates used, the choice of electrolyte has no significant influence on the structural behaviour of the Li_xCoO_2 during the in-situ charge process, as observed in figure 5.

Before commenting on the structural changes observed in Li_xCoO_2 during charge, it is instructive to explore what influence the lower background obtained when using the deuterated electrolyte has on the quality of structural information derived from the diffraction data. Table 1 lists the crystal structure parameters refined using the diffraction data collected from the initial $LiCoO_2$ material in the in-situ cell assembled with normal (H) and deuterated (D) electrolytes. As both datasets were collected for comparable lengths of time, the refined structural parameters and their estimated standard deviations (esds) may be compared: the refined parameters are essentially identical within +/- 1 esd, however the esds are consistently lower for the data collected from the cell using the deuterated electrolyte. The somewhat higher values of the goodness-of-fit parameters, χ^2, R_{wp} and R_p, in the case of the deuterated electrolyte are largely a consequence of the improved quality of the data (higher signal to noise ratio). More importantly, visual inspection of the fit in the *d*-spacing range 2.2 to 2.5 is significantly improved for the cell assembled using deuterated electrolyte with respect to the one assembled with normal electrolyte (see figure 6). Notice that main reflections of $LiCoO_2$ are fitted in this *d*-spacing range: (102), (106) and (101). The use of deuterated electrolyte is clearly shown to be a valuable approach for in-situ neutron diffraction experiments, both from the consistency of the refined values and the improved agreement between the structural model and experimental data (as shown by the difference curve).

3.3 In-situ structural changes of $LiCoO_2$

Previous in-situ studies of $LiCoO_2$ using commercial batteries by Sharma *et al* [45] showed that both forms of $LiCoO_2$; the hexagonal one and the spinel-like phase [46-52], undergo a series of phase transitions during cycling, and it was proposed that the gradual build-up of the spinel-type phase might be a contributing factor to the observed capacity fade within

Li_xCoO_2 based batteries. Rodriguez *et al* [53] determined the variations in the lattice parameters of a $LiCoO_2$-type material as a function of charge state, also in a commercial Li-ion cell, whilst changes in both the lattice parameters and lithium occupancies with repeated cell cycling were shown to be correlated with the degradation of cell performance [54]. In the case of in-situ X-ray powder diffraction studies, Reimers *et al* [55] and Morcrette *et al* [56] showed that Li_xCoO_2 undergoes multiple phase transitions on removal of Li^+. Initially, a single phase material with a rhombohedral structure (named R1) is observed over a small range $1.0 \geq x \geq 0.93$, followed by a two-phase mixture of phases R1 and R2 for $0.93 \geq x \geq 0.73$, where the R2 phase has a similar structure to R1, but differs in *a* and *c* lattice parameters. Single phase R2 forms over the composition range $0.73 \geq x \geq 0.55$, followed by a transformation into a monoclinic phase (named M1) which is stable for $0.55 \geq x \geq 0.45$. The M1 phase then transforms to an R2′ phase for $0.45 \geq x \geq 0.13$ and, whilst the structure of the R2′ phase is similar to that of R2, there is currently no detailed characterisation of the atomic positions.

Figure 7 shows the phase transitions observed in Li_xCoO_2 up to x~0.38, using the in-situ cell filled with deuterated electrolyte. The structural changes at the cathode are clearly identified; in particular, the *d*-spacing of the (110) peak is shifted to lower *d*-spacing whilst the *d*-spacing of the (003) peak is shifted to higher *d* during charge or Li^+ deintercalation from Li_xCoO_2 (the last is not shown since it corresponds to a *d*-spacing range measured using the low angle detector bank 3). The shift in *d*-spacing of these peaks indicate an increase in the lattice parameter *a* and a decrease in lattice parameter *c*. Within the widely accepted picture of fully occupied hexagonal close packed O^{2-} layers, these changes are related to the oxidation of the Co^{3+} species to Co^{4+} and the increased repulsion between adjacent anion layers, respectively, in agreement with previous in-situ XRD work [55,56].

Other phase transitions can be monitored using the single (104) peak observed at 2.005 Å at $x = 1$ which corresponds to R1 in figure 7 but also in figure 8 in the form of a) contour map of the diffraction data with the corresponding changes in the cell voltage, and b) lattice parameter evolution of Li_xCoO_2 as a function of charge. During charge, the (104) peak becomes broader at $x = 0.89$ - 0.80 and then a second peak appears next to it at 2.014 Å, that

corresponds to the R2 phase and is indexed as (104) on a hexagonal unit cell. At Li_xCoO_2 with $x \sim 0.55$ transformation of the R2 phase to the M1 phase occurs. Finally, a new peak appears at ~2.021 Å which can be indexed as (104) using a hexagonal unit cell for R2′, and indicates the formation of the R2′ single phase [55,56]. These structural changes are also supported by the evolution of (107) and (108) peaks which show similar behaviour to that of (104).

In summary, a number of phase changes are visible in the diffraction pattern, with the material adopting pure phase R1 for $1.00 \geq x \geq 0.90$; a mixed phase R1 plus R2 for $0.90 \geq x \geq 0.70$; a single phase R2 region for $0.70 \geq x \geq 0.5$, a mixture of two or more phases including the monoclinic M1 from $0.55 \geq x \geq 0.46$ and, finally the R2' phase from $x = 0.46$ to $x = 0.38$, at which point the cell reached the cut-off voltage of 4.8 V. This sequence of phase changes is consistent with that observed previously [55,56], though with slightly wider phase co-existence ranges, probably due to the relatively low current rate applied to the in-situ cell during the in-situ experiment. Differences in the structural evolution as a function of applied current rate have already been observed in layered rock-salt materials [57] as well as in $LiFePO_4$ [58].

4. Future work.

The electrochemical and neutron powder diffraction data presented in this paper demonstrate that the charge/discharge behaviour of the in-situ cell closely mirrors that of commercial Li-batteries, whilst allowing changes in crystalline phases of the cathode material to be studied in detail. Clearly, this study of the well-known Li_xCoO_2 material illustrates that there is an opportunity to study new lithium-based cathode materials and, indeed candidate anode compounds. The modular nature of the in-situ electrochemical cell allows individual components to be easily exchanged, allowing studies to be performed with different cell geometries and different materials for the current collectors, *etc*. Indeed, the cell has been successfully used for in-situ neutron diffraction studies of nickel-metal-hydride cells [19,22] and to probe rechargeable alkaline iron electrodes [59]. Experiments using sodium based electrodes are planned for the future.

From the technique point-of-view, analysis of the Bragg scattering component of a neutron powder diffraction pattern provides a description of the contents of the unit cell, averaged over time and all the unit cells in the sample. However, within the field of neutron (and, indeed, X-ray) powder diffraction, there is currently a major expansion of interest in so-called 'Pair Distribution Function (PDF)' or 'total scattering' studies. This approach includes the diffuse scattering component, observed as undulations in the background between the Bragg peaks, and can provide information on deviations from the average structure (*i.e*. local defects). However, in the case of in-situ studies, accurate data corrections are required to remove background contributions arising from the instrument and cell and to account for attenuation of the beam by the cell and the sample itself [60,61]. Whilst the increased complexity of the experimental setup has, to date, hampered widespread application of PDF methods within the area of in-situ studies, this is likely to be an area of development in the future.

5. Conclusions.

The technique of neutron powder diffraction offers unique possibilities to study the locations of light species such as H, Li and O within materials containing heavier elements and, as a consequence, provide information central to our understanding of the performance of technologically relevant battery materials. As a contribution to that field, this paper describes an electrochemical cell with a coin cell geometry that has been successfully tested for in-situ neutron diffraction studies of lithium-ion battery materials. Initial studies showed clear structural evolution of $LiCoO_2$ during charge in agreement with previous diffraction studies. Several stages during Li deintercalation from $LiCoO_2$ were identified and correlated with electrochemical data. Significant improvements in the peak-to-background ratio were achieved by replacing normal electrolyte with a deuterated analogue which, in turn, allowed neutron powder diffraction data of good statistical quality to be collected in relatively short counting times. Both from the consistency of the refined values and the best agreement between the structural model and experimental data, the use of deuterated electrolyte is shown to be a valuable approach to in-situ neutron diffraction experiments.

Acknowledgements.

We thank the UK Engineering and Physical Sciences Research Council and Science and Technology Facilities Council for the funding of a PhD studentship to Bo Dong and provision of neutron beamtime.

Tables and Figures captions

Table 1. The refined structural parameters of $LiCoO_2$ derived from diffraction data collected in the in-situ cell with normal (top) and deuterated (bottom) electrolyte.

Figure 1 Schematic diagram of several cells for in-situ electrochemical measurements using neutron radiation, a) and b) are cylindrical designs presented by Bergström *et al* [27] and Sharma *et al* [28,29], respectively; c) and d) are planar designs presented by Novák *et al* [35] and Biendicho *et al* [19] , respectively.

Figure 2 Pictures showing (a) the individual components of the in-situ cell, (b) the assembled cell and (c) the cell with the addition of the neutron absorbing boron nitride shield on the front of the cell.

Figure 3 Pictures showing electrochemical results (a) in the form of cell potential versus capacity for the in-situ electrochemical cell and coin-cell measured in the laboratory using normal (H containing) electrolyte, and b) measured using the electrochemical cell with deuterated electrolyte during in-situ experiment. For all cases, battery components were $LiCoO_2$, graphite and carbon black in the ratio 80:2.5:7.5, Whatman GF/D as glass fibre separator and a 0.38 mm thickness lithium foil.

Figure 4 The neutron powder diffraction patterns collected from $LiCoO_2$ in a vanadium can (red), inside the in-situ cell filled with normal (H) electrolyte (blue) and inside the in-situ cell filled with deuterated electrolyte (green). In the latter two cases, additional reflections from the nickel windows are observed (indicated by the red stars). The weak peaks observed at *d*-spacings of ~1.3Å, ~1.65Å, ~1.80Å and ~2.45Å are associated with the glass fiber separator, carbon and lithium metal within the electrochemical cell.

Figure 5 The evolution of the neutron powder diffraction patterns collected from Li_xCoO_2 during charge, with the sample charged in the in-situ cell and the data collected using high

angle detectors. The improved quality of the diffraction data collected when using deuterated electrolyte (left) rather than protonated electrolyte (right) is clear.

Figure 6 Fitted powder neutron diffraction patterns after Rietveld refinement with data collected from in-situ cells in their initial state filled with normal (H) (top) and deuterated (D) (bottom) electrolyte. The reflections of $LiCoO_2$ and Ni metal are shown by the tick marks. In the case of the Ni peaks, the greater differences arise from preferred orientation within the metal sheets. The insets highlight the *d*-spacing ranges from 2.2Å to 2.5Å.

Figure 7 In-situ neutron diffraction patterns collected from the cell in the Polaris high angle (backscattering) detector bank during battery charge. The battery components were $LiCoO_2$, graphite and carbon black in the ratio 80:2.5:7.5, Whatman GF/D as glass fibre separator, a 0.38mm thick lithium metal anode and 1.5ml of deuterated electrolyte. The labels R1, R2 and R2′ denote the phase of Li_xCoO_2, where *x* is the Li content. The presence of the M1 phase is seen in the appearance of a number of weak peaks in the data collected at x~0.5, such as those seen at *d*-spacings around 2Å. The lower figures highlight the variation of the position of the (110) and (003) reflections during charge.

Figure 8 Contour map showing a) the structural changes of $LiCoO_2$ during charge and, next to it, the voltage profile of the cell as measured during the in-situ experiment, b) variation of the lattice parameter of the rhombohedral R1, R2 and R2′ phases as a function of cathode oxidation (Li content *x*)

Tables and Figures

Atom	Type	*x*	*y*	*z*	Mult.	Occupancy	u_{iso} (×100)
Li1	Li^{+}	0	0	0	3	1	2.6(7)
Co1	Co^{3+}	0	0	0.5	3	1	0.6(3)
O1	O^{2-}	0	0	0.2385(4)	6	1	0.1(1)
$LiCoO_2$, $R\bar{3}m$, *a*=2.8181(2) Å, *c*=14.0618(19) Å, χ^2=2.57, R_{wp}=7.32%, R_p=5.86%							

Atom	Type	*x*	*y*	*z*	Mult.	Occupancy	u_{iso} (×100)
Li1	Li^{+}	0	0	0	3	1	2.1(5)
Co1	Co^{3+}	0	0	0.5	3	1	0.4(2)
O1	O^{2-}	0	0	0.2385(3)	6	1	0.1(1)
$LiCoO_2$, $R\bar{3}m$, *a*=2.8096(1) Å, *c*=14.0183(13) Å, χ^2=5.48, R_{wp}=13.01%, $_p$=15.05%							

Table 1

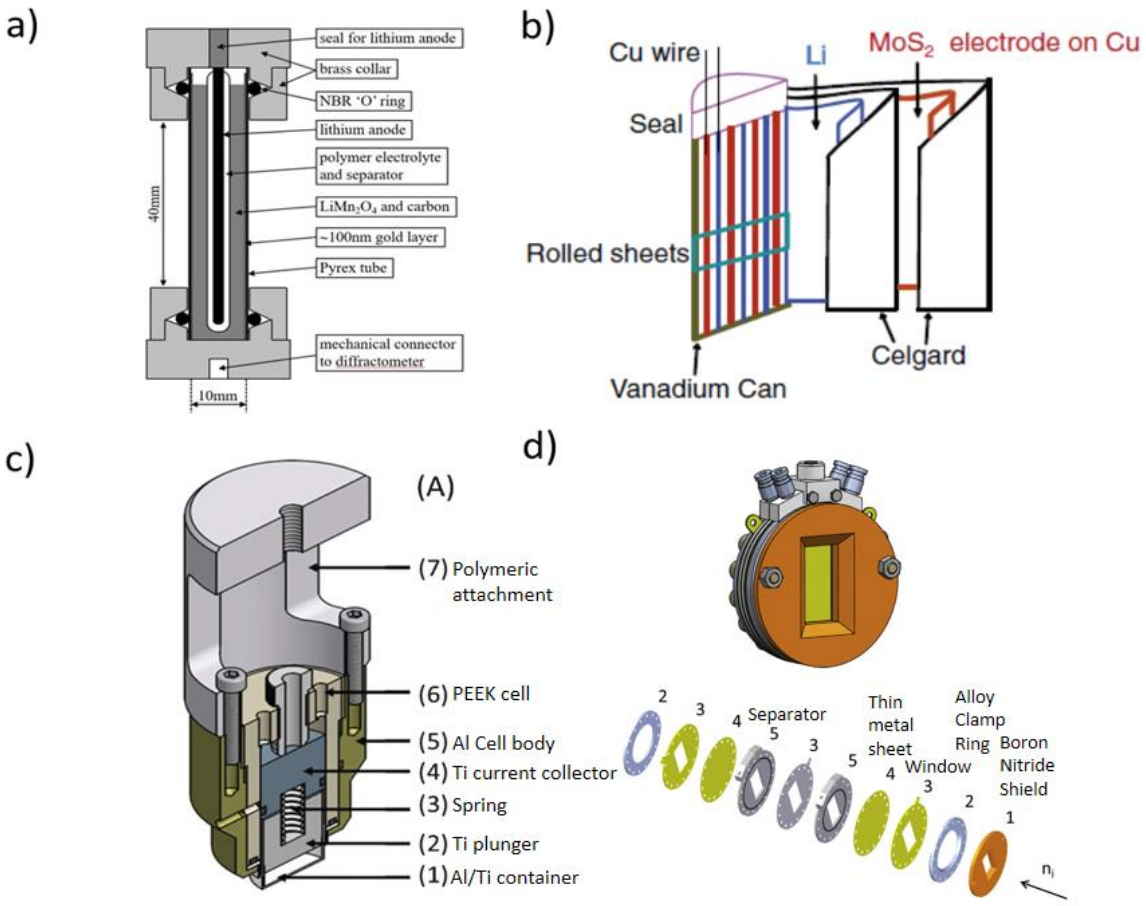
a)
seal for lithium anode
brass collar
NBR 'O' ring
lithium anode
polymer electrolyte and separator
$LiMn_2O_4$ and carbon
~100nm gold layer
Pyrex tube
mechanical connector to diffractometer
40mm
10mm
b)
Cu wire
Li
MoS_2 electrode on Cu
Seal
Rolled sheets
Celgard
Vanadium Can
c)
(A)
(7) Polymeric attachment
(6) PEEK cell
(5) Al Cell body
(4) Ti current collector
(3) Spring
(2) Ti plunger
(1) Al/Ti container
d)
Separator
Thin metal sheet
Window
Alloy Clamp Ring
Boron Nitride Shield
n_i

Figure 1

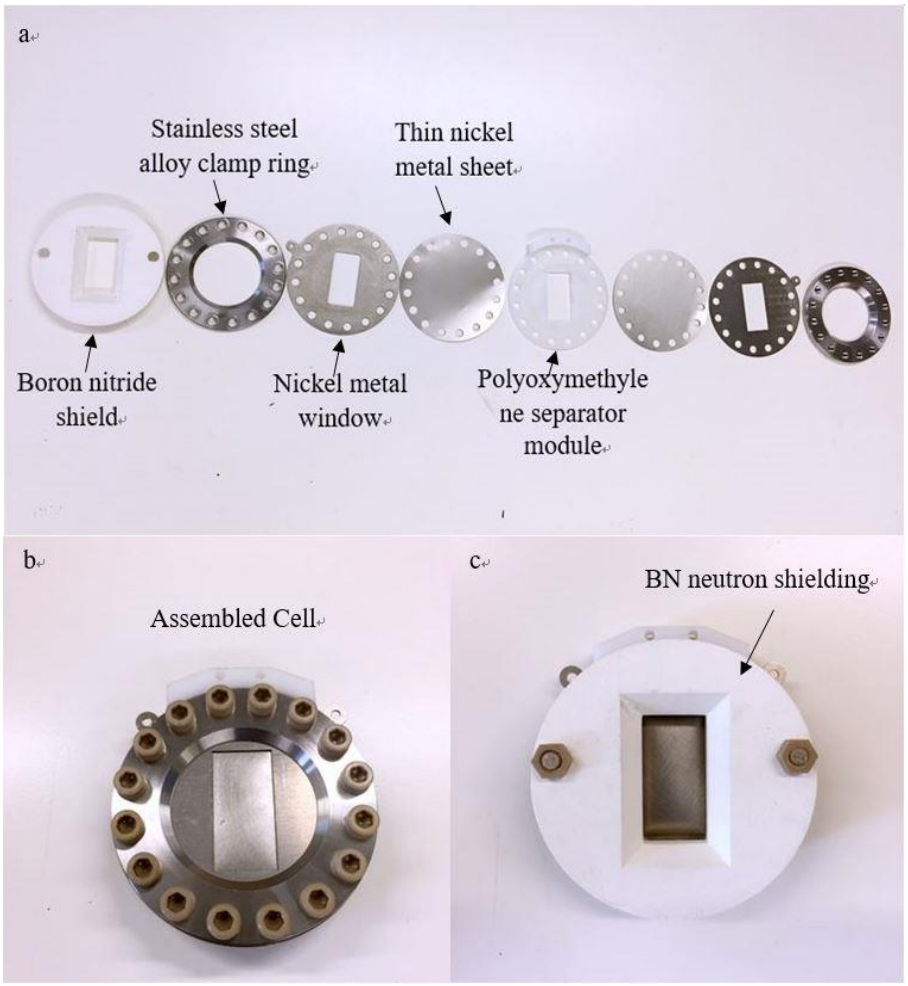
a
Stainless steel alloy clamp ring
Thin nickel metal sheet
Boron nitride shield
Nickel metal window
Polyoxymethylene separator module
b
Assembled Cell
c
BN neutron shielding

Figure 2

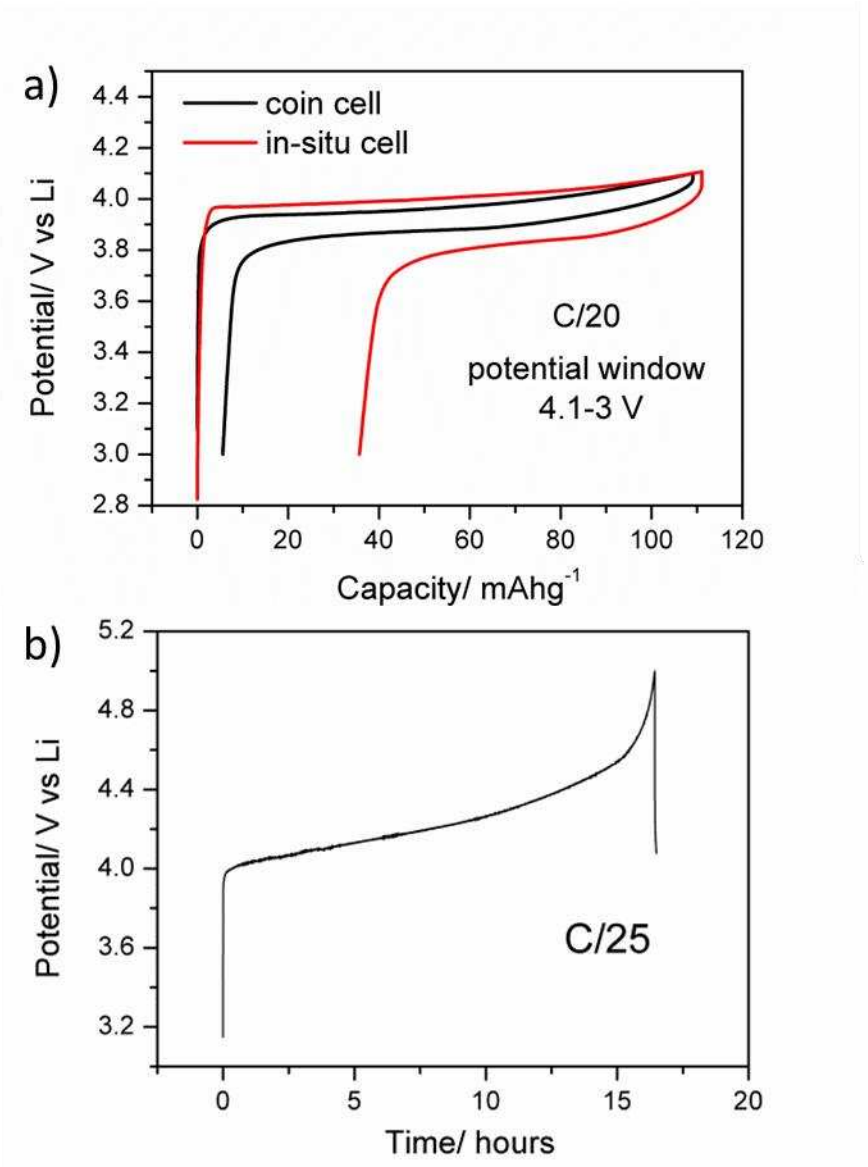
a)
coin cell
in-situ cell
Potential/ V vs Li
Capacity/ mAhg-1
C/20
potential window
4.1-3 V
b)
Potential/ V vs Li
Time/ hours
C/25

Figure 3

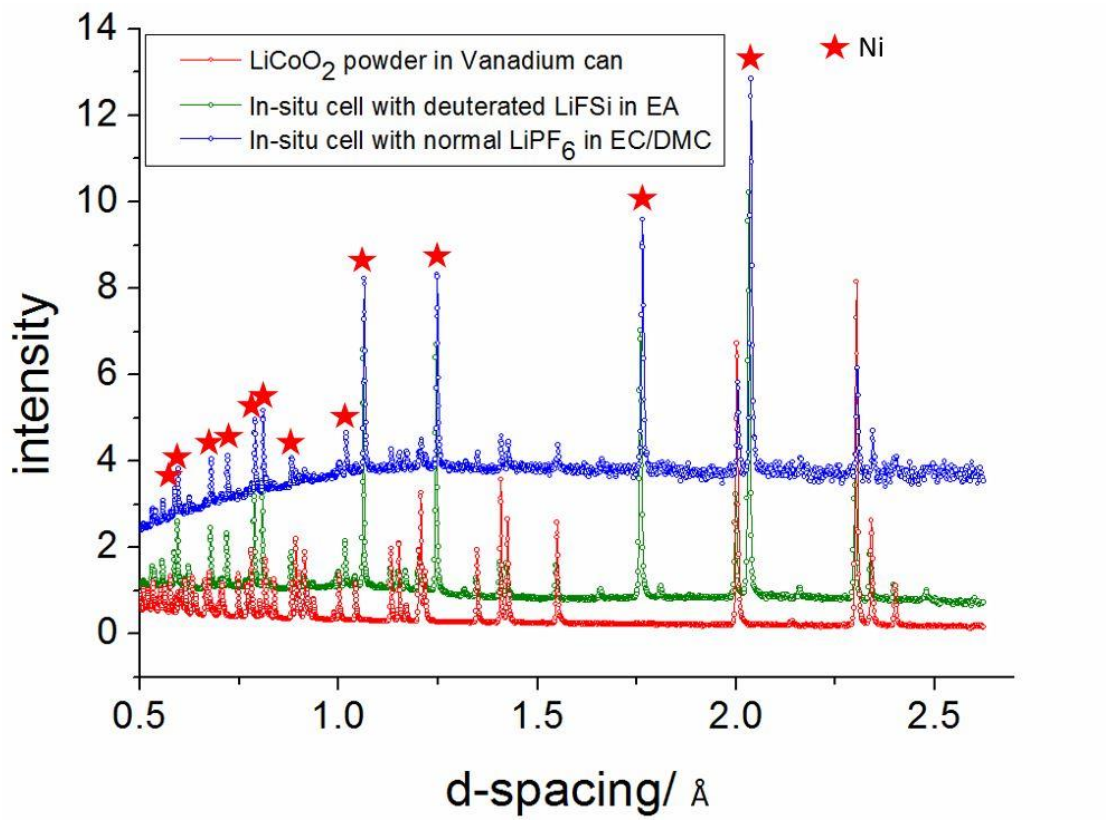
LiCoO2 powder in Vanadium can
In-situ cell with deuterated LiFSi in EA
In-situ cell with normal LiPF6 in EC/DMC
Ni
intensity
d-spacing/ Å
0
2
4
6
8
10
12
14
0.5
1.0
1.5
2.0
2.5

Figure 4

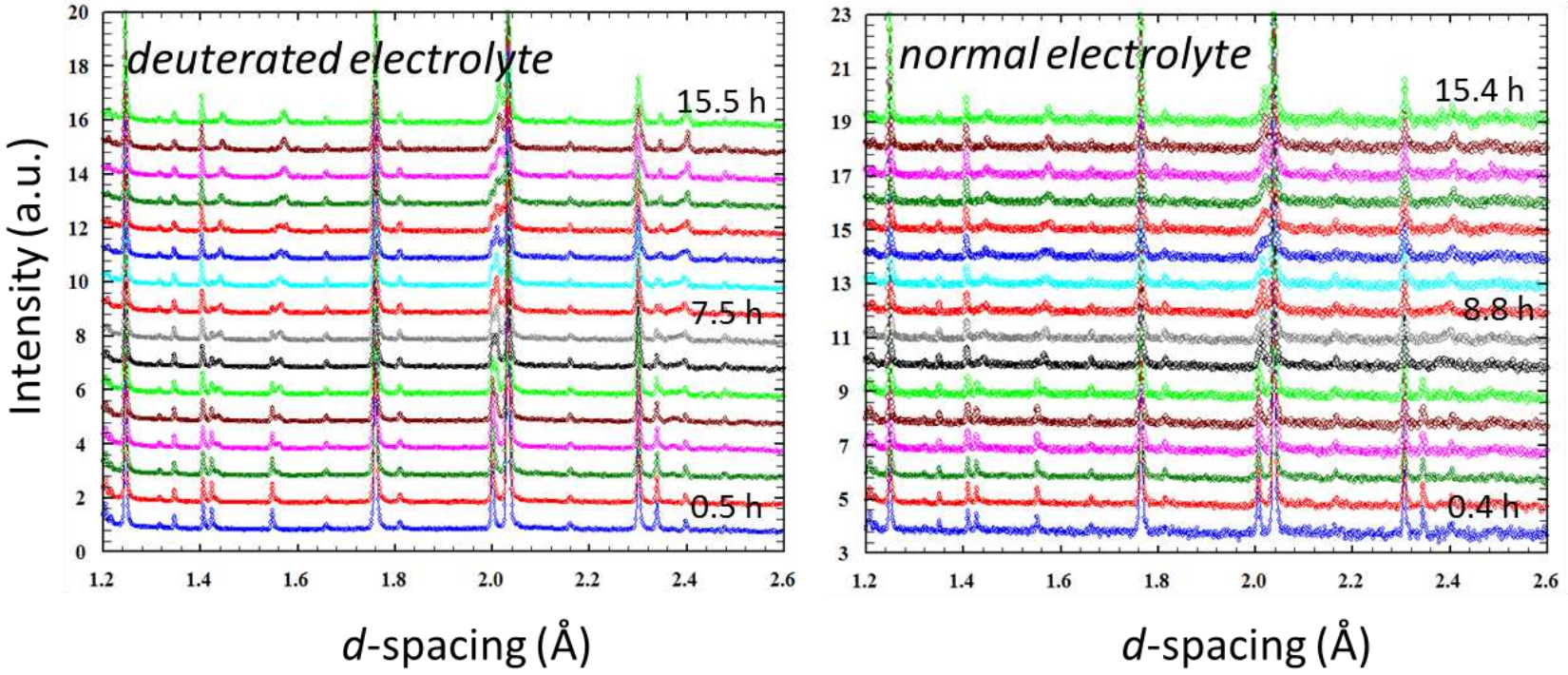
deuterated electrolyte
15.5 h
7.5 h
0.5 h
normal electrolyte
15.4 h
8.8 h
0.4 h
Intensity (a.u.)
d-spacing (Å)
d-spacing (Å)

Figure 5

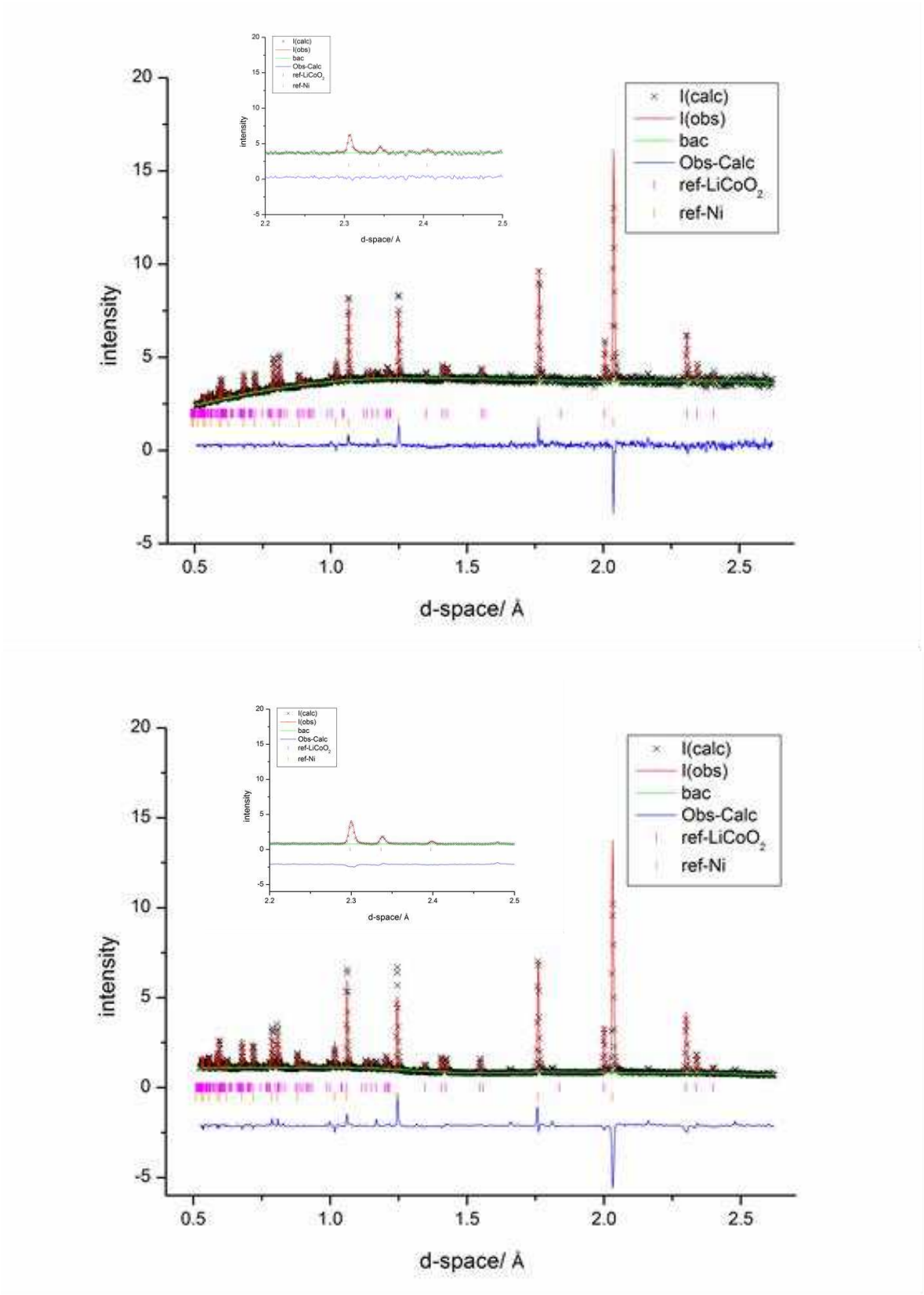
I(calc)
I(obs)
bac
Obs-Calc
ref-LiCoO2
ref-Ni
intensity
d-space/ Å
0.5
1.0
1.5
2.0
2.5
20
15
10
5
0
-5

Figure 6

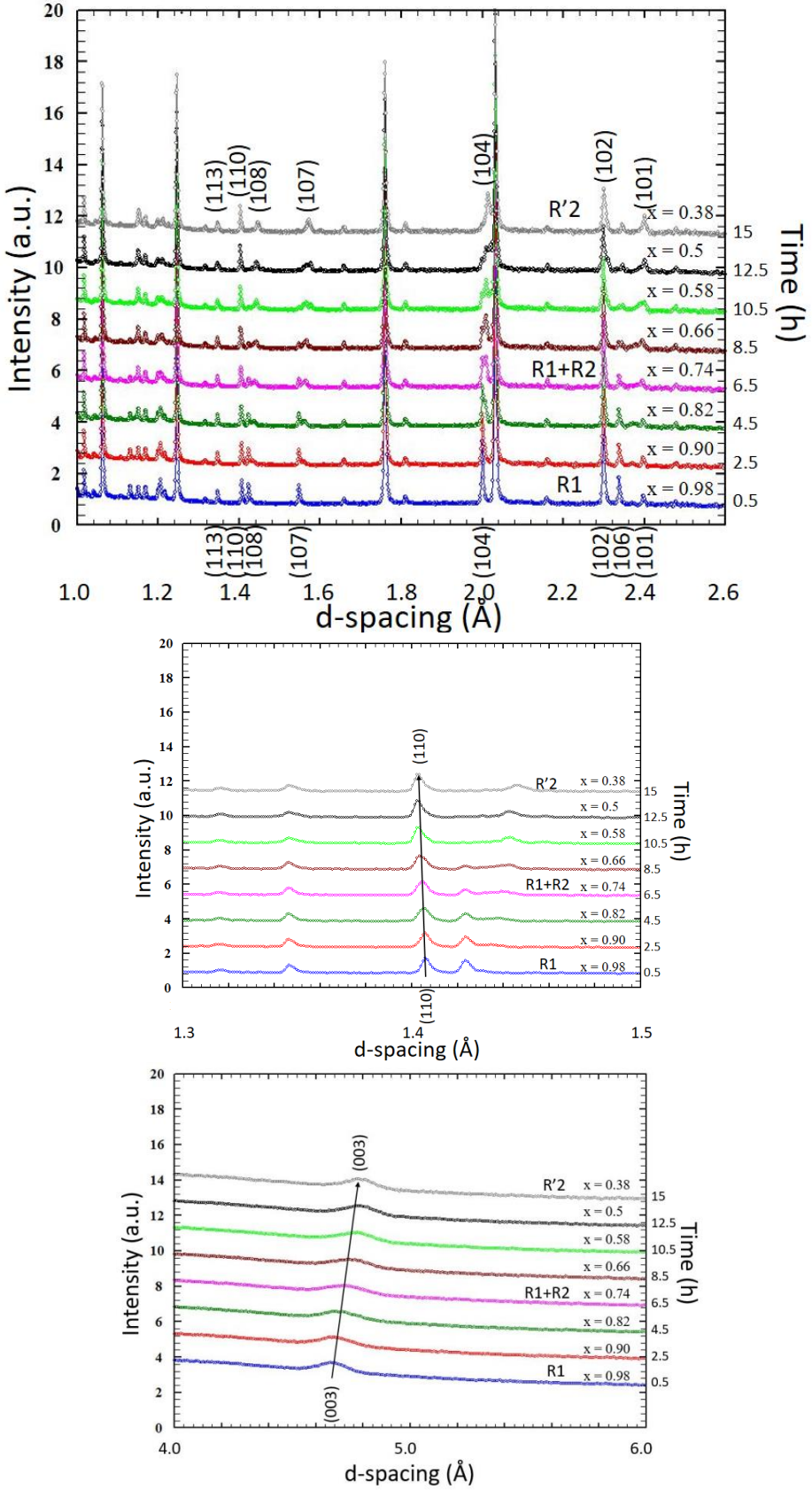
Intensity (a.u.)
d-spacing (Å)
Time (h)
(113)
(110)
(108)
(107)
(104)
(102)
(106)
(101)
R'2
R1+R2
R1
x = 0.38
x = 0.5
x = 0.58
x = 0.66
x = 0.74
x = 0.82
x = 0.90
x = 0.98
(003)

Figure 7

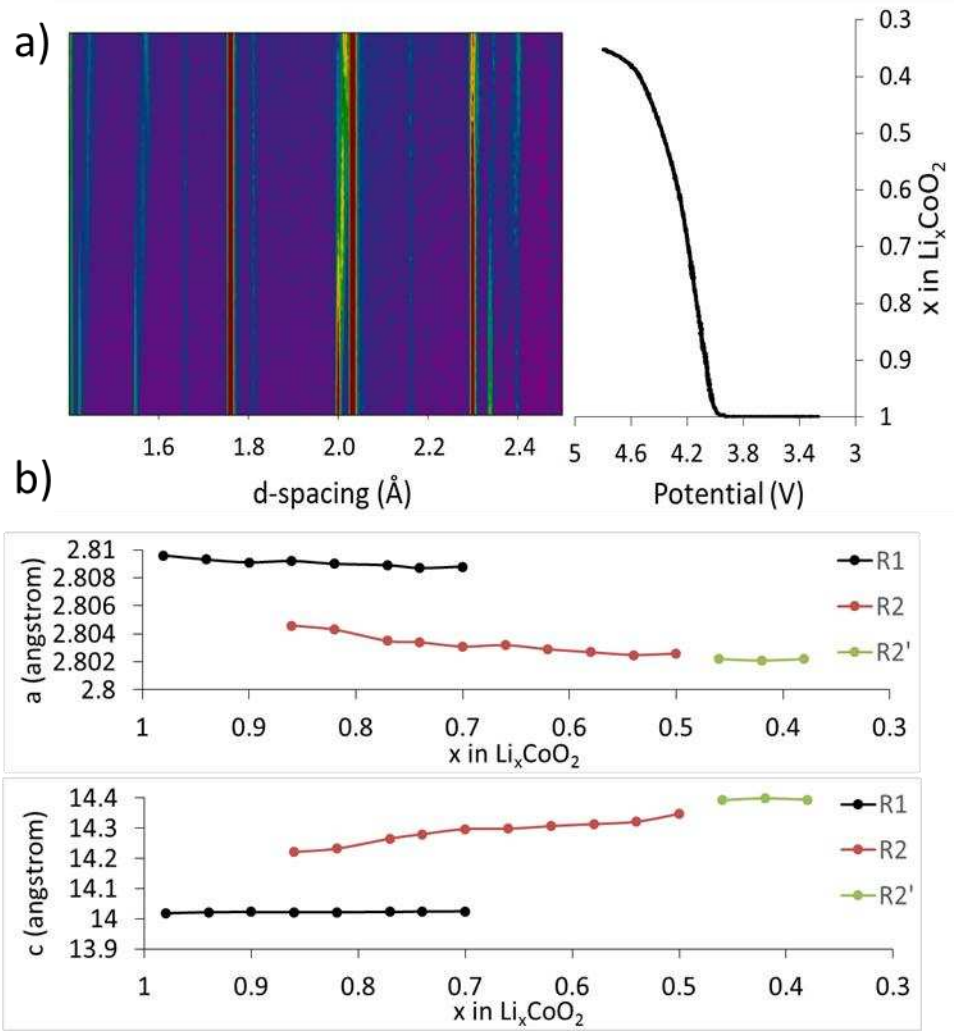
a)
1.6
1.8
2.0
2.2
2.4
d-spacing (Å)
5
4.6
4.2
3.8
3.4
3
Potential (V)
0.3
0.4
0.5
0.6
0.7
0.8
0.9
1
x in Li_xCoO_2
b)
a (angstrom)
2.81
2.808
2.806
2.804
2.802
2.8
1
0.9
0.8
0.7
0.6
0.5
0.4
0.3
x in Li_xCoO_2
R1
R2
R2'
c (angstrom)
14.4
14.3
14.2
14.1
14
13.9
1
0.9
0.8
0.7
0.6
0.5
0.4
0.3
x in Li_xCoO_2
R1
R2
R2'

Figure 8

References

[1] D. Larcher and J.M. Tarascon, "Towards greener and more sustainable batteries for electrical energy storage", *Nature Chem*., **7**, 19-29 (2015).

[2] T. Nagaura and K. Tazawa, "Lithium ion rechrgeable battery", *Prog. Batteries Solar Cells*, **9**, 209-217 (1990).

[3] R.-S. Kühnel, N. Böckenfeld, S. Passerini, M. Winter and A. Balducci, "Mixtures of ionic liquid and organic carbonate as electrolyte with improved safety and performance for rechargeable lithium batteries", *Electrochim. Acta*, **56**(11), 4092-4099 (2011).

[4] A. Lewandowski and A. Swiderska-Mocek, "Ionic liquids as electrolyte for Li-ion batteries- An overview of electrochemical studies", *J. Power Sources*, **194**(2), 601-609 (2009).

[5] J.M. Tarascon and M. Armand, "Issues and challenges facing rechargeable lithium batteries", *Nature*, **414**, 359-367 (2001).

[6] K. Edström, T. Gustafsson and J.O. Thomas, "The cathode-electrolyte interface in the Li-ion battery", *Electrochim. Acta*, **50**(2-3), 397-403 (2004).

[7] M. Broussely, Ph. Biensan, F. Bonhomme, Ph. Blanchard, S. Herreyre, K. Nechev and R.J. Staniewicz, "Main aging mechanism in Li ion batteries", *J. Power Sources*, 146, 90-96 (2005).

[8] N. Nitta, F. Wu, J.T. Lee and G. Yushin, "Li-ion battery materials: present and future", *Materials Today*, **18**(5), 252-264 (2015).

[9] C. Liu, Z.G. Neale and G. Cao, "Understanding electrochemical potentials of cathode materials in rechargeable batteries", *Materials Today*, **19**(2), 109-123 (2016).

[10] P.P.R.M.L. Harks, F.M. Mulder and P.H.L. Notten, "In-situ methods for Li-ion battery research: A review of recent developments", J. Power Sources, **288**, 92-105 (2015).

[11] G.J. Kearley and V.K. Peterson, "Neutron applications in materials for energy", Springer (2015).

[12] T.C. Hansen and H. Kohlmann, "Chemical reactions followed by in-situ neutron powder diffraction", *Z. Anorg. Allg. Chem*., **640**, 3044-3063 (2014).

[13] S.W. Lovesey, "Theory of neutron scattering from condensed matter. I. Nuclear scattering", vol. 1, Oxford University Press (1986).

[14] S.W. Lovesey, "Theory of neutron scattering from condensed matter. II. Polarization effects and magnetic scattering", vol. 1, Oxford University Press (1986).

[15] B.T.M. Willis (ed.), "Chemical applications of thermal neutron scattering", Oxford University Press (1973).

[16] B.T.M. Willis and C.J. Carlile, "Experimental neutron scattering ", Oxford University Press (2009).

[17] C.G. Windsor, "Pulsed neutron scattering", John Wiley and Sons, Ltd. (1981).

[18] V.F. Sears, "Neutron scattering lengths and cross sections", *Neutron News*, **3**, 26 - 37 (1992).

[19] J.J. Biendicho, M. Roberts, C. Offer, D. Noréus, E. Widenkvist, R.I. Smith, G. Svensson, K. Edström, S.T. Norberg, S.G. Eriksson and S. Hull, "New in-situ neutron diffraction cell for electrode materials", *J. Power Sources*, **248**, 900-904 (2014).

[20] M. Roberts, J.J. Biendicho, S. Hull, P. Beran, T. Gustafsson, G. Svensson and K. Edström, "Design of a new lithium ion battery test cell for in-situ neutron diffraction measurements", *J. Power Sources*, **226**, 249-255 (2013).

[21] B. Vadlamani, K. An, M. Jagannathan and K.S. Ravi Chandran, "An in-situ electrochemical cell for neutron diffraction studies of phase transitions in small volume electrodes of Li-ion batteries", *J. Electrochem. Soc.,* **161**(10), A1731-A1741 (2014).

[22] J.J. Biendicho, M. Roberts, D. Noréus, U. Lagerqvist, R.I. Smith, G. Svensson, S.T. Norberg, S.G. Eriksson and S. Hull, "In-situ investigation of commercial $Ni(OH)_2$ and $LaNi_5$-based electrodes by neutron powder diffraction", *J. Mater. Res.,* **30**, 407-416 (2015).

[23] W.R. Brant, M. Roberts, T. Gustafsson, J.J. Biendicho, S. Hull, H. Ehrenberg, K. Edström and S. Schmid, "A large format in operando wound cell for analyzing the structural dynamics of lithium insertion materials", *J. Power Sources*, **336**, 279-285 (2016).

[24] R. Petibon, J. Li, N. Sharma, W.K. Pang, V. Peterson and J.R. Dahn, "The use of deuterated ethyl acetate in highly concentrated electrolyte as a low-cost solvent for in situ neutron diffraction measurements of Li-ion battery electrodes", *Electrochim. Acta*, **174**, 417-423 (2015).

[25] N. Sharma, D.H. Yu, Z. Zhu, Y. Wu and V.K. Peterson, "In operando neutron diffraction study of the temperature and current rate-dependent phase evolution of $LiFePO_4$ in a commercial battery", *J. Power Sources*, **342**, 562-569 (2017).

[26] D. Goonetilleke, J.C. Pramudita, M. Hagan, O.K. Al Bahri, W.K. Pang, V.K. Peterson, J. Groot, H. Berg and N. Sharma, "Correlating cycling history with structural evolution in commercial 26650 batteries using in operando neutron powder diffraction", *J. Power Source*s, **343**, 446-457 (2017).

[27] Ö. Bergstöm, A.M. Andersson, K. Edström and T. Gustafsson, "A neutron diffraction cell for studying lithium-insertion processes in electrode materials", *J. Appl. Cryst*., **31**, 823-825 (1998).

[28] G. Du, N. Sharma, V.K. Peterson, J.A. Kimpton, D. Jia and Z. Guo, "Br-doped $Li_4Ti_5O_{12}$ and composite TiO_2 anodes for Li-ion batteries: synchrotron X-ray and in situ neutron diffraction studies", *Adv. Funct. Mater*., **21**, 3990-3997 (2011).

[29] N. Sharma, G. Du, A.J. Studer, Z. Guo and V.K. Peterson, "In-situ neutron diffraction study of the MoS_2 anode using a custom-built Li-ion battery", *Solid State Ionics*, **199-200**, 37-43 (2011).

[30] W.R. Brant M. Roberts, T. Gustafsson, J.J. Biendicho, S. Hull, H. Ehrenberg, K. Edström and S. Schmid, "A large format in operando wound cell for analyzing the structural dynamics of lithium insertion materials", *J. Power Sources*, **336**, 279-285 (2016).

[31] L. Boulet-Roblin, P. Borel, D. Sheptyakov, C. Tessier, P. Novák and C. Villevieille, "Operando neutron powder diffraction using cylindrical cell design: the case of $LiNi_{0.5}Mn_{1.5}O_4$ vs graphite", *J. Phys. Chem. C*, **120**, 17268-17273 (2016).

[32] L. Boulet-Roblin, D. Sheptyakov, P. Borel, C. Tessier, P. Novak and C. Villevieille, "Crystal structure evolution via operando neutron diffraction during long-term cycling of costumized 5 V full Li-ion cylindrical cells $LiNi_{0.5}Mn_{1.5}O_4$ vs. graphite", *J. Mater. Chem. A*, **DOI: 10.1039/C7TA07917F.**

[33] J. Li, R. Petibon, S. Glazier, N. Sharma, W.K. Pang, V.K. Peterson and J.R. Dahn, "In-situ neutron diffraction study of a high voltage $Li(Ni_{0.42}Mn_{0.42}Co_{0.16})O_2$/Graphite pouch cell", *Electrochim. Acta*, **180**, 234-240 (2015).

[34] W.K. Pang and V.K. Peterson, "A custom battery for operando neutron powder diffraction studies of electrode structure", *J. Appl. Crystallogr*., **48**, 280-290 (2015).

[35] V.A. Godbole, M. Heb, C. Villevielle, H. Kaiser, J.-F. Colins and P. Novák, "Circular in situ neutron powder diffraction cell for study of reaction mechanism in electrode materials for Li-ion batteries", *RSC Adv*., **3**, 757-763 (2013).

[36] A. Vadlamani, K. An, M. Jagannathan and K.S. Ravi Chandran, "An in-situ electrochemical cell for neutron diffraction studies of phase transitions in small volume electrodes of Li-ion batteries", *J. Electrochem. Soc*., **161**(10), A1731-A1741 (2014).

[37] M. Bianchini, J.B. Leriche, J.-L. Laborier, L. Gendrin, E. Suard, L. Croguennec and C. Masquelier, "A new matrix electro-chemical cell for Rietveld refinements of in-situ or operando neutron powder diffraction data", *J. Electrochem. Soc.*, **160**(11), A2176-A2183 (2013).

[38] F. Rosciano, M. Holzapfel, W. Scheifele and P. Novák, "A novel electrochemical cell for in-situ neutron diffraction studies of electrode materials for lithium-ion batteries", *J. Appl. Cryst.*, **41**, 690-694 (2008).

[39] S. Hull, R.I. Smith, W.I.F. David, A.C. Hannon, J. Mayers and R. Cywinski, "The Polaris powder diffractometer at ISIS", *Physica B*, **180-181**, 1000-1002 (1992).

[40] A.C. Larson and R.B. Von Dreele: Report LA-UR-86-748 (Los Alamos National Laboratory, Los Alamos, NM87545, 1990).

[41] Inorganic Crystal Structure Database, http://cds.dl.ac.uk

[42] G.G. Amatucci, J.M. Tarascon and L.C. Klein, "CoO_2, the end member of the Li_xCoO_2 solid solution", *J. Electrochem. Soc*., **143**, 1114-1123 (1996).

[43] K. Mizushima, P.C. Jones, P.J. Wiseman and J.B. Goodenough, "Li_xCoO_2 ($0<x<1$); a new cathode material for batteries of high energy density", *Mater. Res. Bull*., **15**, 783-789 (1980).

[44] T. Ohzuku and A. Ueda, "Solid state redox reactions of $LiCoO_2$ (R-3m) for 4 volt secondary cells", *J. Electrochem. Soc*., **141**, 2972-2977 (1994).

[45] N. Sharma, V.K. Peterson, M.M. Elcombe, M. Avdeev, A.J. Studer, N. Blagojevic, R. Yusoff and N. Kamarulzaman, "Structural changes in a commercial lithium-ion battery during electrochemical cycling: An in-situ neutron diffraction study", *J. Power Sources*, **195**, 8258-8266 (2010).

[46] B. Garcia, P. Barboux, F. Ribot, A. Kahn-Harari, L. Mazerolles and N. Baffier, "The structure of low temperature crystallized $LiCoO_2$", *Solid State Ionic*s, **80**, 111-118 (1995).

[47] R.J. Gummow, D.C. Liles and M.M. Thackeray, "Spinel versus layered structures for lithium cobalt oxide synthesised at 400°C", *Mater. Res. Bull*., **28**, 235-246 (1993).

[48] R.J. Gummow, D.C. Liles, M.M. Thackeray and W.I.F. David, "A reinvestigation of the structures of lithium cobalt oxides with neutron diffraction data", *Mater. Res. Bull*., **28,** 1177-1184 (1993).

[49] R.J. Gummow and M.M. Thackeray, "Lithium cobalt nickel oxide cathode materials prepared at 400oC for rechargeable lithium batteries", *Solid State Ionics*, **53**, 681-687 (1992).

[50] R.J. Gummow, M.M. Thackeray, W.I.F. David and S. Hull, "Structure and electrochemistry of lithium cobalt oxide synthesized at 400°C", *Mater. Res. Bull*., **27**, 327-337 (1992).

[51] E. Rossen, J.N. Reimers and J.R. Dahn, "Synthesis and electrochemistry of spinel LT-$LiCoO_2$", *Solid State Ionics*, **62,** 53-60 (1993).

[52] Y. Shao-Horn, S.A. Hackney, C.S. Johnson, A.J. Kahaian and M.M. Thackeray, "Structural features of low-temperature $LiCoO_2$ and acid-delithiated products", J. *Solid State Chem*., **140**, 116-127 (1998).

[53] M.A. Rodriguez, D. Ingersoll, S.C. Vogel and D.J. Williams, "Simultaneous in situ neutron diffraction studies of the anode and cathode in a lithium-ion cell", *Electrochem. Solid State Lett.*, **7**, A8-A10 (2004).

[54] O. Dolotko, A. Senyshyn, M.J. Muhlbauer, K. Nikolowski, F. Scheiba and H. Ehrenberg, "Fatigue process in Li-ion cells: An in situ combined neutron diffraction and electrochemical study", *J. Electrochem. Soc*., **159**, A2082-A2088 (2012).

[55] J.N. Reimers and J.R. Dahn, "Electrochemical and in-situ X-ray diffraction studies of lithium intercalation in LixCoO2", *J. Electrochem. Soc*., **139**, 2091-2097 (1992).

[56] M. Morcrette, Y. Chabre, G. Vaughan, G. Amatucci, J.B. Leriche, S. Patoux, C. Masquelier and J.M. Tarascon, "In situ X-ray diffraction techniques as a powerful tool to study battery electrode materials", *Electrochimica Acta*, **47**, 3137-3149 (2002).

[57] Y.-N. Zhou, J.-L. Yue, E. Hu, H. Li, L. Gu, K.-W. Nam, S.-M. Bak, X. Yu, J. Liu, J. Bai, E. Dooryhee, Z.-W. Fu and X.-Q. Yang, "High-rate charging induced intermediate phases and structural changes of layer-structured cathode for lithium-ion batteries", *Adv. Energy Mater.*, **6**, 1600597 (2016).

[58] Y. Koyama, T. Uyama, Y. Orikasa, T. Naka, H. Komatsu, K. Schimode, H. Murayama, K. Fukuda, H. Arai, E. Matsubara, Y. Uchimoto and Z. Ogumi, "Hidden two-step phase transition and competing reactions pathways in $LiFePO_4$", *Chem. Mater.*, **29**, 2855-2863 (2017).

[59] M. Chamoun, B. Skarman, H. Vidarsson, R.I. Smith, S. Hull, M. Lelis, D. Milcius and D. Noreus, "Stannate increases hydrogen evolution overpotential on rechargeable alkaline iron electrodes", *J. Electrochem. So*c., **164**, A1251-A1257 (2017).

[60] A.C. Hannon, W.S. Howells and A.K. Soper, "ATLAS. A suite of programs for the analysis of time-of-flight neutron diffraction data from liquid and amorphous samples", *Inst. Phys. Conf. Ser.*, **193-211** (1990).

[61] M.A. Howe, R.L. McGreevy and W.S. Howells, "The analysis of liquid structure data from time-of-flight neutron diffractometry", *J. Phys.: Condens. Matter*, **1**, 3433-3451 (1989).